Fracture Mechanics of Concrete and Concrete Structures -
Assessment, Durability, Monitoring and Retrofitting of Concrete Structures- B. H. Oh, et al. (eds)
 ISBN 978-89-5708-181-5

Crack detection using embedded cement-based piezoelectric sensor

Y. Lu & Z. Li
Department of Civil and Environmental Engineering, Hong Kong University of Science & Technology, China

ABSTRACT: In this paper, the new methodology to detect the crack propagation in concrete will be presented. The methodology will employ newly developed cement-based piezoelectric sensors that can be embedded into a concrete structure. The new sensors have the advantages of good compatibility with concrete, broad flat response spectrum, and good durability. By employing cement-based piezoelectric sensors, different mode of fractures have been studied, including tension, shear and mixed mode. The experiments results show that such new sensors can detect the formation of micro-crack, propagation of micro or macro crack, and different mode of failure.

1 INTRODUCTION

Early researches on the AE analysis mainly rely on the traditional parameter (accumulated events numbers, event rate etc.) elevation. These parameters variation and trend have long been used to predict the onset of damage or sever failure (Reymond 1983, Hamstad 1986, Li & Shah 1994). And the AE source locations have also been estimated on 2-D planar graph by using derived partial differential equations (Li & Shah 1994). Moreover, the recorded AE waveforms have been further used to interpret the mode of micro-fracture by a seismic moment tensor (Li 1996). With the development of modern signal processing technique, AE measurement and evaluation researches have focused on manipulating the advanced technique, such as the frequency domain analysis and wavelet analysis, for fracture mode classification of AE signals from composites materials (Yoon et al. 2000).

In this paper, cement-based piezoelectric composites sensors with improved sensitivity and better frequency domain performance were used to detect the damage process of two kinds of static loading conditions. The objective of this research is to verify the feasibility of damage monitoring for concrete by using the brand new piezoelectric sensors array and the signal-based monitoring technique. 3-D localization of AE sources was introduced based on the embedded cement-based piezo sensors array. Further more, the defined signal-based fracture energy index, together with various frequency components of the detected AE signals were figured out to investigate the variation of crack condition throughout concrete fracture process.

2 CEMENT-BASED PIEZOELECTRIC COMPOSITE SENSORS ARRAY

The compatibility of the piezoelectric material and matrix material is a critical issue in health monitoring since that it greatly affects the performance of the piezoelectric material in its ability of detection and actuation of acoustic waves. If the compatibility can not meet the request, the detecting sensitivity and SNR (signal to noisy ratio) will be unsatisfactory. In civil engineering, concrete is dominant construction material. However, there exists relatively large difference on stiffness, linear elastic modulus and the acoustic impedance between concrete and metal. The traditional sensors which are especially designed for metal materials may not be suitable for concrete material for achieving optimal performance. In order to ensure perfect compatibility between passive detecting utility and matrix material, three aspects of issues should be paid attention to, including good coupling, matching of the acoustic impedance and consistency. In 2002 Li et al. found that it is possible to overcome these problems using a brand new cement-based piezoelectric composite which has the acoustic impedance value close to that of the concrete matrix by adjusting the mix proportion of ceramic material and portland cement particles. This composite improved the damping characteristic of the sensing element when embedded into the concrete (the acoustic impedance of the cement-based piezo composite is approximately 10) resulting in flat and broad frequency domain response, and the sensitivity enhanced accordingly. Nowadays, cement-based piezo composites with six kinds of connectivity patterns have been developed. In this experiment, cement-based piezoelectric composites of 0-3 connectivity

Figure 1. The 0-3 cement-based piezoelectric composite sensor.

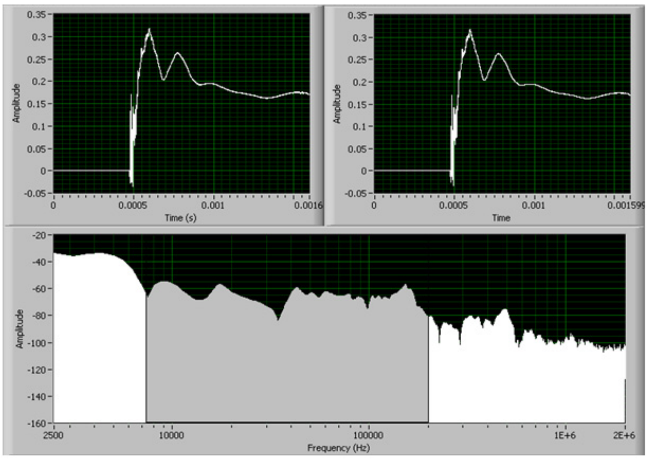

Figure 2. The time domain (top) & frequency domain (bottom) response of the cement-based piezo sensor subjected to Hsu pencil lead break (shadow area indicate the flat frequency response range).

patterns were employed as the constituent materials of the piezoelectric sensor (see Fig 1.)

The piezo sensors own a broad and flat frequency domain response which covers the frequency region of AE from concrete cracks. The sensitivity calibration results are shown in Figure 2.

In each test, totally eight piezoelectric sensors were embedded at the corners of the concrete specimen (see Fig. 3) to constitute the detecting array for health monitoring of concrete specimens during loading. During the tests, at least 5 sensors (or 4 un-coplanar sensors) were required to identify and record the AE effectively in order to localize the AE sources correctly and satisfactorily. A C++ program was coded to carry the job.

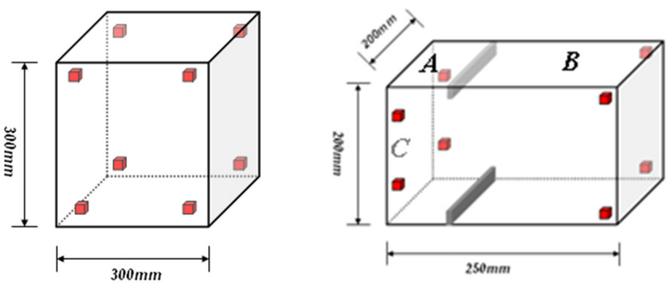

Figure 3. The detecting array arrangement inside of the test specimen (left: splitting, right: direct-shear test).

The 3-D locations could be calculated using the time differences of the first arrival (TDOA) from different monitoring channels of an acquisition system. It had been theoretically proved that in order to ensure iteration converges on the source location of AE, the least required number of channels shall be guaranteed (two channels for linear localization, three for planar localization and four for volumetric localization). Additionally, accurate arrival time determination method must also be available. In our experiments, a 128-point band-pass FIR filter (20 KHZ~300 KHz) with hamming windows was used to smooth the original signal waveform detected by the sensors array in order to efficiently make the arrival point sharper and easily be identified.

3 HOME-PROGRAMMED DECLIN HEALTH MONITORING SYSTEM

The elementary function block of the DEcLIN system is illustrated in Figure 4. The system consists of 0-3 cement-based piezoelectric sensors presented previously, voltage pre-amplifier, 8-channel data acquisition hardware and corresponding software.

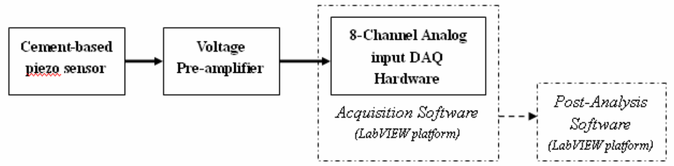

Figure 4. The block diagram of DEcLIN system.

The maximum sampling rate of the designed acquisition system is 10MHz which is capable of perfectly reconstructing the signals within 2MHz frequency region with negligible distortion, and it is changeable depending on the monitoring duration and information precision required. The software is divided into two components: signal acquisition software and post-analysis software (Fig. 5.) in order to efficiently prevent the two individual processes from interfering with each other and occupying excessive RAM storage space. And advanced signal-based health monitoring analysis, together with traditional parameter-based health monitoring analysis, can be realized based on this data transmission and processing framework.

4 EXPERIMENTAL SETUP

4.1 *Splitting test*

The objective of Splitting test was to induce a tensile crack dominant failure mode on concrete material specimen. The detected AE signals were used to extract the signal-based information on the fracture process

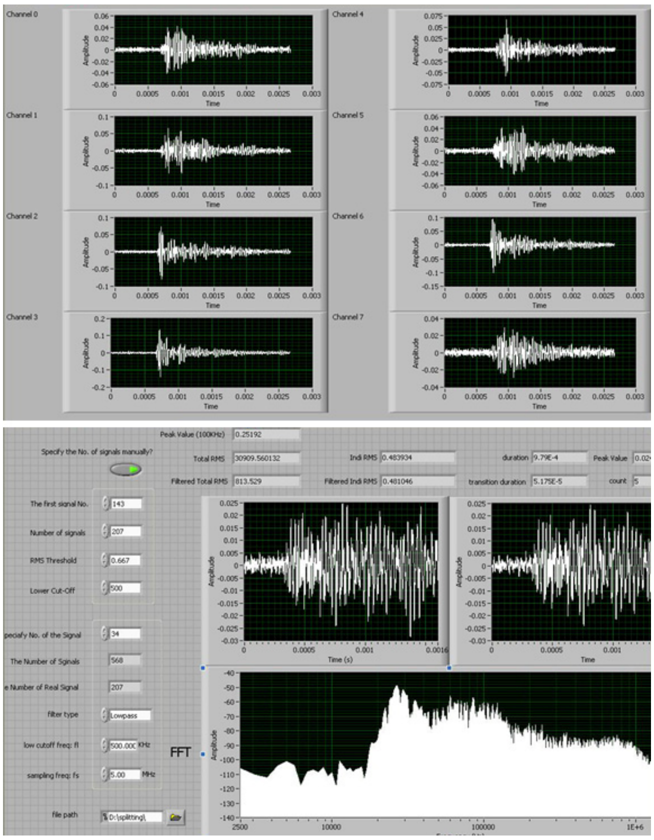

Figure 5. The acquisition (top) and post-analysis (bottom) DEclin software.

of test and analyze the variation trend of tensile crack induced AE sources. The test procedure and apparatus were designed conforming to ASTM C496-96, while the dimension of concrete specimen is a 300mm*300mm*300mm cube (see Fig. 3) which is convenient for sensors to be embedded in the corners forming a detection array. The mixture proportions used in preparing the specimens (Splitting & Direct-shear) are listed in Table 1.

Table 1. The mixture proportion of the concrete specimen in the experiments.

Material	cement	water	sand	SP
Mortar	1	0.5	1.8	0.2%

Two LVDTs of 10mm working range were mounted on the front and back side of the concrete cube in horizontal direction respectively to measure the horizontal displacement due to expanding in the center. The displacement values form LVDTs were also fed back to control the loading rate for guaranteeing a stable loading process.

4.2 *Direct-shear Test*

The objective of Direct-shear test was to induce a shear crack dominant failure mode on concrete specimen. Similarly, the detected AE signals were used to extract the signal-based information and summarize the variation trend of shear crack-induced AE sources. ASTM standard D5607-02 (Standard Test Method for Performing Laboratory Direct Shear Strength Tests of Rock Specimens under Constant Normal Force) was introduced as reference for apparatus and test procedure design. The dimension of concrete specimen is a 250mm long, 200mm wide and 200mm high cuboid. A 40mm depth and 2.5mm width notches were pre-casted into both the top and bottom faces of the cuboid with a distance of 50mm to the face C (see Fig. 3.). The cement-based piezo-electric sensors array arrangement is a little different to that of Splitting test due to the presence of induced notches and large compressive stress on the face A. The sensors supposed to be at the corners right below face A were embedded with a distance of 40mm for safety and reliability reason. LVDTs of 25mm working range were installed on the top of the concrete cuboid to measure the vertical downward displacement relative to the stationary reference plate of the loading machine.

5 DAMAGE PROCESS MONITORING RESULTS AND ANALYSIS

5.1 *Splitting test*

Prior to the applied load level reached around 82% of ultimate load capacity, the concrete specimen stayed in the pre-burst region which is the time period with the characteristic of limited number of AEN (accumulated event number) recorded and a stable but low-level of ER (event rate) accompanied by compared with the following fracture processes. This characteristic was defined as the criteria of recognizing the pre-burst region (Lu & Li 2008). In our experiment, this pre-burst region was further divided into two subsets marked A & B accordingly with 24% of ultimate load as the division boundary. Afterwards, once the load level was over 82% of ultimate load, a major crack emerged suddenly and the specimen was spitted apart by a brittle crack in the middle plane. The corresponding time period was called the burst region featured the significant rise of AEN (see Fig. 6.) recorded with a sharp rise slope and a narrow pulse recorded on the ER diagram (see Fig. 7). We also further divided the burst region into regimes C, D & E for detailed analysis of fracture process.

In regime A, the concrete materials deformed essentially linear elastically, with extraordinary few AE being recorded by the DEcLIN health monitoring system. From the 3-D localization graph of regime A B & E in Figure 8, it can be found that the AE sources dispersedly scattered close to the middle plane where the high tensile stress concentrated. The AE sources in this regime ought to be micro-cracks primarily stemming from the casting defects, free water evaporation voids and other pre-existing C-S-H weak links in the hydrated concrete materials. In regime

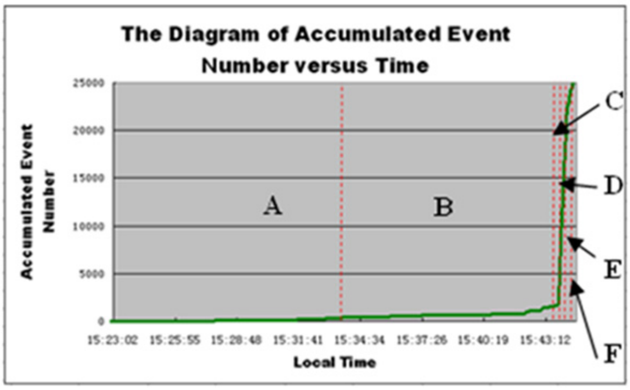

Figure 6. The AEN diagram of Splitting Test (red broken line as the regime boundary).

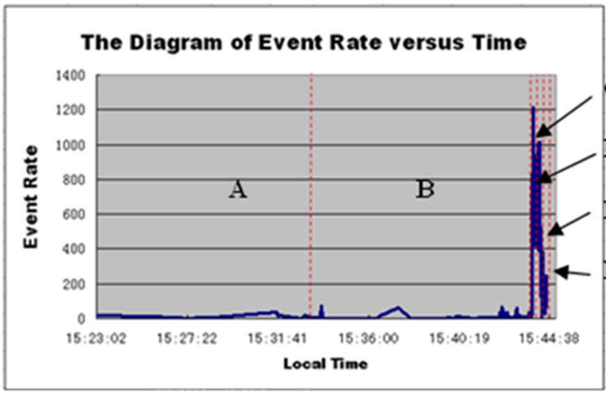

Figure 7. The ER diagram of Splitting Test (red broken line as the regime boundary).

B, the AEN began to increase a little bit, but was still in the low level. The AE sources tended to start to be close together towards the center of the specimen, which is called the micro-crack localization in literature. And it was often observed when a major crack was likely to occur (Li & Shah 1994) as the applied load level was close enough to the ultimate load. After the load level was over 80%of ultimate load, both AEN value and ER value grew up abruptly. From regime D, we observed that most of the AE sources concentrated at the center of the specimens showing that a brittle major crack appeared and propagated quickly at the center with a large number of AE sources recorded simultaneously. The 3-D localization diagram of regime E is shown as a representative. It is found that the splitting fracture process of concrete materials is a brittle process with a major crack propagating from inside towards outside very rapidly. Meanwhile it is clearly observed that the brittle process has a very obvious and rapid micro-crack localization behavior from 3-D localization of AE.

5.2 *Direct-shear Test*

The fracture process of the Direct-Shear test was found out to be in an even more brittle way than that of Splitting test. Prior to the load level reaching approximately 96% of ultimate load capacity, AE signals Were seldom detected based on the results of AEN

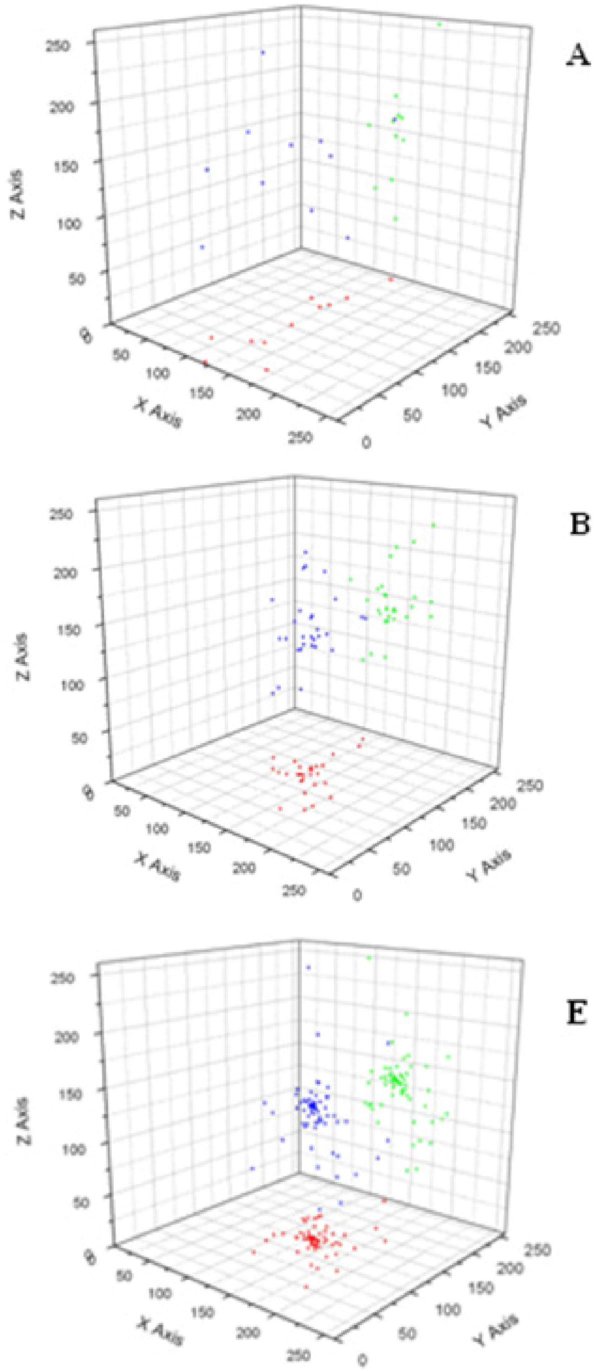

Figure 8. The 3-D localization of Splitting Test in respective regime (with projections on the XY plane and XZ plane).

(see Fig. 9) and ER (see Fig. 10). It was called the pre-burst region similar to that of Splitting test. And it was subdivided into two subsets marked A & B accordingly with 76% of ultimate load as the division boundary so as to study the fracture process in detail. At the moment the load level was over 96% of ultimate load, an explicit curved cracking accompanied by several tiny cracking appeared rapidly from the tip of the top notch towards the bottom face. We classify it as the burst region because of the significant increasing of the AEN and ER as defined previously, and we subdivided this burst region into regimes C, D & E. Additionally, we define a post-burst region after the burst region and marked it regime F. In this region, we could observe that both AEN and ER had a trend of slowing down indicating that the AE activities were not active any more. The concrete specimen was considered failed at this moment.

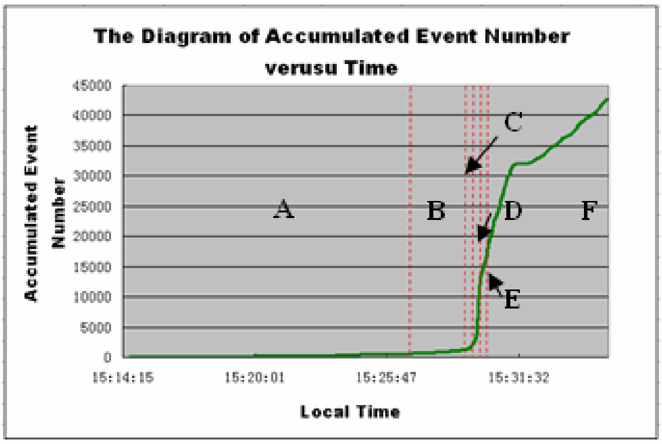

Figure 9. The AEN diagram of Direct-shear Test (red broken line as the regime boundary).

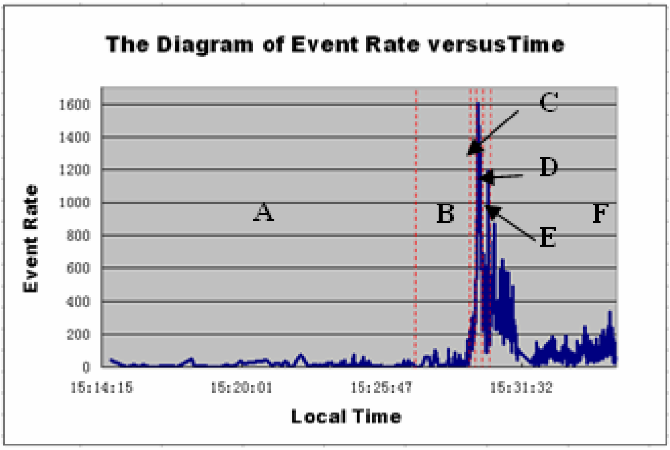

Figure 10. The ER diagram of Direct-shear Test (red broken line as the regime boundary).

In regime A, the concrete materials deformed essentially linear elastically, and the AE signals received were negligible. From the 3-D localization graph of the corresponding regime in Fig 11, it could be found that the AE sources scattered mainly in the top and bottom region close to the notch area due to the local stress concentration induced at tip of the notch. In regime B, the AEN began to increase slowly. And more micro-crack began to appear mainly at the upper body of the specimen. In regime D, the micro-crack localization phenomena became very obvious and started to move downwards in a curved trail. The 3-D localization trail is found to be consistent with the eye observation of the surface cracking. It turns out to be a very rapid crack propagation process given that the time period of the two regimes is very short. In regime E & F, the localization phenomena disappeared and the AE sources were found out back to scatter around the entire curved seems that after a major crack was formed, the applied

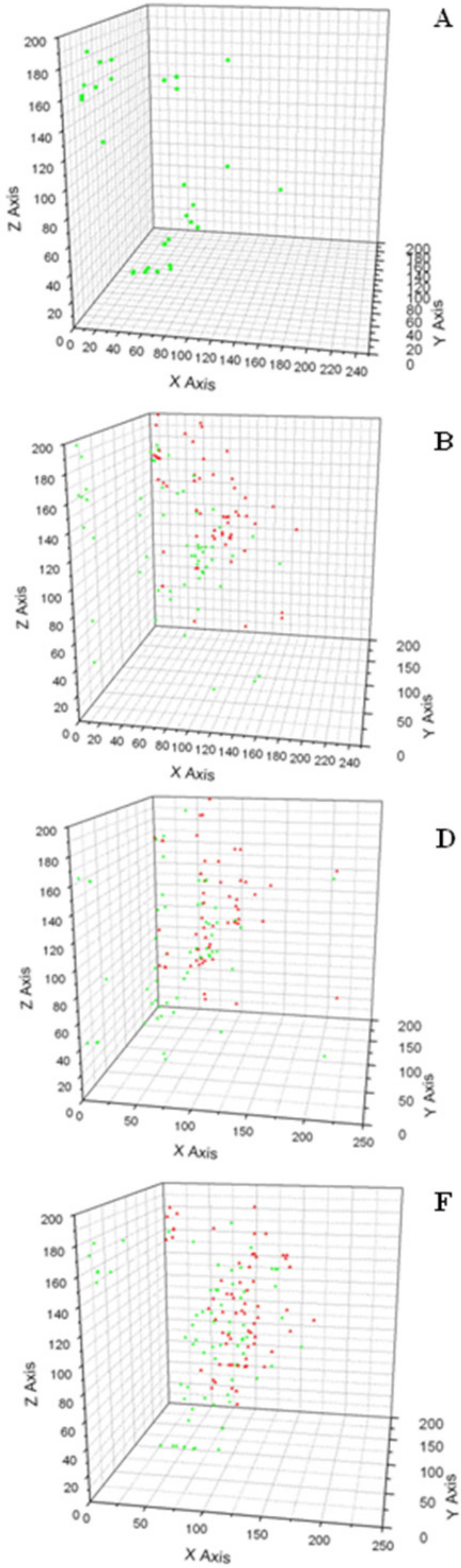

Figure 11. The 3-D localization of Direct-shear Test in respective regime (with projections on the XZ plane).

force was redistributed inside the concrete because of the emergence of a large crack mouth opening. And the friction of the crack surface began to become an important source of AE as shown in the 3-D diagram of regime F.

6 SIGNAL-BASED FRACTURE ENERGY INDEX & FREQUENCY DOMAIN COMPONENTS EVOLUTION

Since AE signal is usually considered as a function of varying amplitude through time, it seems reasonable that to use the area under the *f(x)* enveloping curve as a good approximate measurement of the energy of an AE signal. The total energy of a signal, *f(x)*, is thus defined as the sum of squared module:

$$\varepsilon_f \overset{\Delta}{=} \sum_{x=0}^{N-1} \left| f(x) \right|^2 \tag{1}$$

x refers to the discrete time point of the detected signal.

N represents the total number of the discrete time points.

In digital signal processing, physical unit of the signal energy is routinely discarded, and the signals are renormalized whenever convenient. Therefore, the defined signal-based fracture energy index of an AE signal *f(x)* is introduced as the square root of its total signal energy:

$$\left\| f(x) \right\| \overset{\Delta}{=} \sqrt{\varepsilon_f} = \sqrt{\sum_{x=0}^{N-1} \left| f(x) \right|^2} \tag{2}$$

In experiments, AE signals were caught by the cement-based piezoelectric sensors array and calculated by the home-programmed DEcLIN system using formula (2) to evaluate the signal-based fracture energy index. The 8-channel sensors array was employed simultaneously to record the AE waveforms from 8 directions in order to minimize the probability of energy index error due to micro-cracks and singular points in the wave propagation paths. The signal-based fracture energy index evolution diagrams for Splitting test & Direct-shear test are illustrated in Figures 12,13.

In Figure 12, it was found that the variation of signal-based fracture energy index during the Splitting test is quite similar to the variation of ER in Splitting. Before the applied load level approached 82% of the ultimate load, the fracture energy released was very limited and the variation was negligible. Once 82% overcame, the fracture energy released increased very quickly and reached the peak the same time as ER, indicating the AE activities were turning into the most active period, i.e. micro-crack localization period. A major crack was formed, and the specimen failed consequently. The fracture energy released in the failure minute consists around 71% of the total energy released indicating that this damage process was definitely brittle. Figure 13 shows the variation of energy during Direct-shear test. Similarly, the fracture energy released before 96% of ultimate load was relatively small and had little variation. However, after 96% of ultimate, the energy released increased dramatically. The damage process was turned out to be even more brittle than that of Splitting test. And the energy released in the failure minute occupied more than 72% of the total energy released before failure.

In Figures 12,13 the peak amplitude evolution of 40 KHz, 100KHZ and 200 KHz components were also plotted to investigate the variation of individual frequency components of AE signals detected during fracture process. These single frequency components were obtained by filtering the detected original signals using Butterworth 5-order band-pass filter with center frequency of 40 KHZ, 100 KHz and 200 KHz respectively and bandwidth 30KHz (gain -3 dB, about 0.707 relative to peak). From Figures 12,13 it was seen that the variation of 40 KHz, 100 KHz and 200 KHz all bearing relatively the same trend with the evolution of fracture energy index stated previously. However, by comparing the relative frequency component magnitude variation ratio in each test,

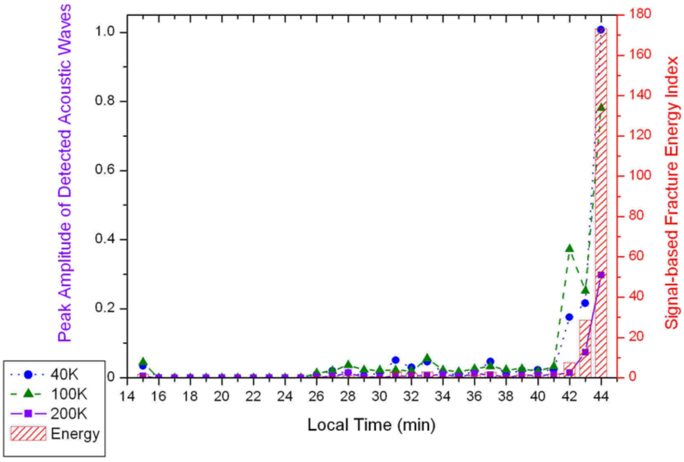

Figure 12. The signal-based fracture energy index of Splitting Test.

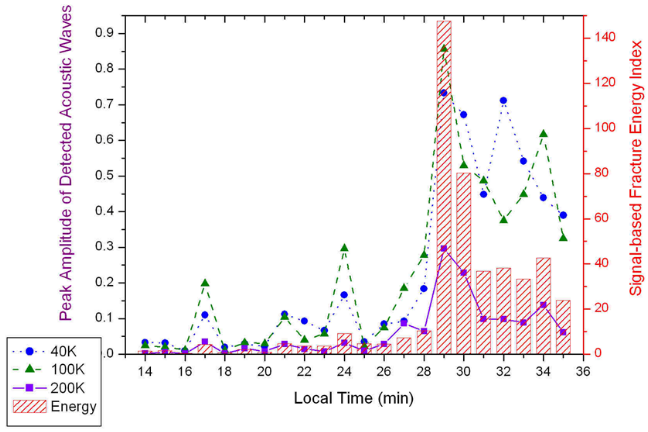

Figure 13. The signal-based fracture energy index of Direct-shear Test.

the 100 KHz component seemed to contribute more to the variation of detected signal-based fracture energy index regardless of static loading conditions. Clearly, the frequency components around 100 KHz of acoustic signals detected must be closely related to the variation of micro-crack behaviors during loading. Moreover, micro-crack condition under static loading could be further investigated by studying the relationship between the frequency domain components and the micro-crack mechanism. From the wavelet analysis of AE signals of concrete cracks, it was observed that 100 KHz frequency components were exactly within the transition boundary zone of P-wave & S-wave components of an AE. This transition boundary was found to be not fixed but within a region of 75 KHz~107 KHz (see Fig. 14). Therefore, when the 100 KHz components became very active, it was believed that there existed some significant changes in the micro-crack behaviors of concrete at that time.

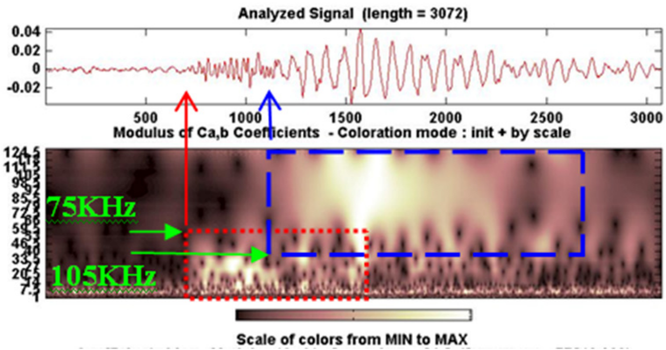

Figure 14. Wavelet transform of a typical AE waveform from Splitting test (the red arrow indicates the arrival of P-wave, and the blue indicates the arrival of S-wave).

7 CONCLUSION

In this paper, different modes of fractures of concrete have been studied using embedded cement-based piezoelectric sensors array. 3-D localization and signal-based fracture energy index evolution was employed to analyze the damage process and evaluate the condition of the specimen under static loading. The following conclusions could be drawn from the study.

(1) The new sensors have the advantages of good compatibility with concrete, broad flat response spectrum, and good durability. And it is capable of monitoring damage processes under static loadings. The AE generated from the concrete cracks could be clearly detected with high sensitivity and SNR.
(2) 3-D localization of AE sources was estimated and illustrated according to the corresponding defined loading stage. Together with the results of AEN and ER, the fracture process under loading could clearly be recognized and investigated.
(3) A signal-based fracture energy index was introduced to quantitatively evaluate the fracture energy released throughout the fracture process. By using band pass filtering, it was found that each frequency component of AE signals contributed differently to the total energy index and varied with time.

ACKNOWLEDGEMENT

The support from China Ministry of Science & Technology under 2009CB623200 and Hong Kong Research Grant Council under N_HKUST637/9 is greatly appreciated.

REFERENCE

Carpinteri A. et al.2007. Structural Damage Diagnosis and Life-time Assessment by Acoustic Emission Monitoring. Engineering Fracture Mechanics, 74, pp273-289
Eric N. L. & Lucie B.2002. Experiments to Relate Acoustic Emission Energy to Fracture Energy of Concrete. Journal of Engineering Mechanics, Vol.128, No.6, June 1
Faming L. & Zongjin L.2000. Acoustic Emission Monitoring of Fracture of Fiber-Reinforced Concrete in Tension. ACI Materials Journal Vol.97, No.6 November-December
Jochen H. K. et al.2005. Strategies for reliable automatic onset time picking of acoustic emissions and of ultrasound signals in concrete. Ultrasonics 43 pp538-546
Ohtsu M. et al.1991. Determination of Crack Locations, Type and Orientation in Concrete Structures by Acoustic Emission. Magazine of Concrete Research, 43, No.155, June, pp127-134
Ohtsu M.1996. The History and Development of Acoustic Emission in Concrete Engineering. Magazine of Concrete Research, 48, No.17, Dec., pp321-330
Raghu P. & Vidya S.2008. Relationship between AE Energy and Fracture Energy of Plain Concrete Beams: Experimental Study. Journal of Materials in Civil Engineering, Vol.20, March 1
Youyuan L. & Zongjin L.2008. Cement-based piezoelectric sensor for acoustic emission detection in concrete structures. Proceedings of the 11th International Conference on Engineering, Science, Construction, and Operations in Challenging Environments
Zongjin L.1996. Micro-crack Characterization in Concrete under Uniaxial Tension. Magazine of Concrete Research, 48, No.176, Sep pp219-228
Zongjin L. et al.2000. P-wave Arrival Determination and AE Characterization of Concrete. Journal of Engineering Mechanics, Vol.126, No.2, February